Int. J. Solids Structures Vol. 18, No. 12, pp. 1083–1102, 1982
Printed in Great Britain.

0020-7683/82/121083-20$03.00/0
Pergamon Press

RESONANCES IN THE SONAR CROSS SECTIONS OF COATED SPHERICAL SHELLS

G. C. GAUNAURD and A. KALNINS†
Naval Surface Weapons Center, R-43 White Oak, Silver Spring, MD 20910, U.S.A.

(*Received* 4 *November* 1981; *in revised form* 22 *March* 1982)

Abstract—We have constructed an analytical model from first principles that will permit the prediction of the sound fields scattered by spherical elastic shells covered with a layer of viscoelastic materials, which contain an inner fluid different from the outer fluid surrounding the laminated structure. This model is constructed as a sound/structure boundary-value-problem which accounts for sound fields interior to the submerged shell. The model is exact insofar as the equations of linear elasticity/visco-elasticity can be considered accurate descriptors of the vibrations of the laminated structure. Any conceivable damping level present in the viscoelastic layer, can be quantitatively accounted for in the predictions. We have successfuly separated the shape factors (or backgrounds) from the re-radiated (or resonance) portions that combine to make up each modal contribution to the structure's backscattering cross section, in the manner of the Resonance Scattering Theory (RST). We have quantitatively analyzed the damping effect the coating has on the modal resonances, either considering each mode individually or after adding them all together in the cross section. Sound penetration into this target takes place through the discrete spectral windows centered at the (rigid, in this instance) resonances of the fluid-loaded structure, and we show how each such resonance produces each one of the rapid oscillations present in the sonar cross section. We display many calculations of the (summed) cross section, of the modes or partial waves contained within it, and of the backgrounds (shape factors) and resonance (re-radiated) portions which makeup each mode. This is another realistically modelled situation for a penetrable structure, that successfuly fits in the neighborhood of acoustic behavior near the idealized extreme of rigid impenetrability, where the RST is most useful.

INTRODUCTION

The interaction of sound waves with elastic spherical shells immersed in fluids is a well plowed subject that seems to have started with the pioneering work of Junger[1–3]. The in-vacuo vibrations of layered spherical shells were studied by Kalnins[4] who later extended and reviewed[5] the whole subject of vibrating shell theories excluding the acoustic interaction aspects. A variety of shell theories have been introduced to describe the behavior of fluid-loaded spherical shells[1, 6, 7] while some investigators have analyzed the transmission and/or reflection of sound waves through thick spherical shells by means of the exact equations of linear elasticity[8].

Some of the comprehensive work of Hickling studied the echoes returned by submerged spherical shells[9–11] theoretically, experimentally, at low and high frequencies, and even using frequency-modulated sound pulses as incident waves. Monostatic and bistatic cross-sections of *partially* insonified submerged spheres were recently studied using the physical optics method[12] and in another instance, by means of an exact theory of finite sound beams[13] which are techniques easily extended to the case of spherical *shells*. Transient interactions of plane sound waves with spherical shells were analyzed by Huang[14] although most of the available work on sound scattering by elastic shells has used incident continuous waves. We are not aware of the existence of much work dealing with any type of incident continuous acoustic wave that is not plane.

If the spherical shell is made of sound-absorbing (i.e. viscoelastic) material, one finds only a limited amount of pertinent publications. For the case of "impedance covered" spherical shells, some work has been reported in the foreign literature[15a], where in depth studies on multilayered shells have been available for some time[15b]. A detailed scattering analysis of impedance covered spheres has also been recently published at this Center[16].

The investigation of low-frequency seismic wave propagation through the Earth's crust has led seismologists to develop extensive layered spherical shell models[17] of the Earth that sometimes can be made to account for thousands of layers. These models have obvious uses in

†Also at the Mechanical Engineering and Mechanics Department, Lehigh University, Bethlehem, PA 18015, U.S.A.

the analysis of scattered fields from large layered spheres. If some of the upper layers are liquid and some of the bottom ones are made to represent solid, possibly porous sediments, then the models serve to study the ocean bottom[18, 19] from the acoustically reflected field.

Very simple absorbing situations such as an absorbing sphere in water under planewave insonification, have been briefly studied in superficial ways[20, 21] and even in an erroneous way[22]. Air-filled *cylindrical* shells covered with viscoelastic layers, submerged in water and insonified at beam aspects by plane sound waves, have been the subject of some recent analysis both at low frequencies[23, 24] as well as at high[25]. The effect of small fluid-filled cavities sometimes present in the outer viscoelastic layer has also been studied under the light of the new Resonance Scattering Theory for cavities in solids[26]. This Resonance Theory has also been used to study some aspects of the reflection of plane sound waves from metallic shells in water[27]. It now follows that a basic problem that still remains to be posed and solved is that of a submerged air-filled spherical elastic shell covered with a layer of visocelastic material, and subject to plane-wave insonification. In the present paper we will analyze this sound/structure interaction problem as well as the effect the absorptive characteristics of the coating have on the backscattered cross-section or "echo" of the spherically layered structure. The absorbing layer is assumed to have a homogeneous composition and viscous coefficients of known or given values. This viscoelastic layer is also assumed to be ideally bonded to the elastic shell. Anyone familiar with the processes usually followed to bond rubber to steel[28] is aware of the difficulties involved in this assumption. The resulting complex boundary-value problem will be studied by means of the exact equations of viscoelasticity or elasticity that govern the coating and the shell motions, respectively[29]. The solutions in each one of the layers are coupled at the interfaces between them, by suitable boundary conditions to be introduced in due time. Therefore, we have developed an *exact* model for the complete analysis of the sound/structure interaction problem, insofar as the equations of linear elasticity/viscoelasticity describe the motion of the bilaminar shell structure. All absorption levels that could possibly be present in the outer absorbing layer, are accounted for by means of this approach. Since this approach and solution are exact, any approximation introduced later on to characterize the shell motions will have to be compared to the present solution which will become the norm or calibration standard. Suitable shell theories could later be used to simplify the present approach. We have also analyzed the modal contributions that add up to the sonar cross-section in the manner typical of the Resonance Scattering Theory[30, 31] in order to separate the shape and re-radiation components of each of its constituent normal modes; a process that is quite enlightening in the understanding of the scattering mechanism taking place around and inside the coated shell. Finally, we have analyzed some aspects of the effect the absorption damping in the outer coating layer has on the shell and on the coating resonances which cause the re-radiation.

VISCOELASTICITY BACKGROUND

The field equations of linear dynamic viscoelasticity in terms of displacements and in the Kelvin–Voigt viscoelastic model are

$$\left[1+\frac{\mu_v}{\mu_e}\frac{\partial}{\partial t}\right]\nabla^2\bar{u}+\left[\frac{\lambda_e+\mu_e}{\mu_e}\right]\left[1+\frac{\lambda_v+\mu_v}{\lambda_e+\mu_e}\right]\frac{\partial}{\partial t}\nabla(\nabla\cdot\bar{u})=\frac{1}{c_s^2}\frac{\partial^2\bar{u}}{\partial t^2} \tag{1}$$

where λ_e, μ_e are the elastic Lamé constants, λ_v, μ_v are their viscous counterparts, and $c_s=(\mu_e/\rho)^{1/2}$ is the speed of shear waves in the viscoelastic medium. The above relations reduce to the standard Navier equations of elasticity in the absence of viscosity. For the axially symmetric case in spherical coordinates, of interest to this paper, the above equations take the following particular form

$$\nabla_{r\theta}^2 u_r-\frac{2u_r}{r^2}-\frac{2}{r^2}\frac{\partial u_\theta}{\partial\theta}-\frac{2u_\theta\cot\theta}{r^2}+\left[1+\frac{\lambda_e-i\omega\lambda_v}{\mu_e-i\omega\theta_v}\right]\frac{\partial\Delta}{\partial r}+\kappa_s^2 u_r=0$$

$$\nabla_{r\theta}^2 u_\theta-\frac{2}{r^2}\frac{\partial u_r}{\partial\theta}-\frac{u_\theta}{r^2\sin^2\theta}+\left[1+\frac{\lambda_e-i\omega\lambda_v}{\mu_e-i\omega\mu_v}\right]\frac{1}{r}\frac{\partial\Delta}{\partial\theta}+\kappa_s^2 u_\theta=0 \tag{2}$$

where

$$\nabla_{r\theta}^2 = \frac{\partial^2}{\partial r^2} + \frac{2}{r}\frac{\partial}{\partial r} + \frac{1}{r^2}\frac{\partial^2}{\partial \theta^2} + \frac{\cot\theta}{r^2}\frac{\partial}{\partial \theta} \tag{3}$$

$$\Delta = \frac{\partial u_r}{\partial r} + \frac{2u_r}{r} + \frac{1}{r}\frac{\partial u_\theta}{\partial \theta} + \frac{u_\theta}{r}\cot\theta \tag{4}$$

$$\kappa_s^2 = \rho\omega^2/(\mu_e - i\omega\mu_v) \tag{5}$$

and where time-dependence of the form $e^{-i\omega t}$ has been assumed wherever pertinent.

We have shown earlier [29] that eqns (2) are automatically satisfied provided that we introduce two scalar potentials, ϕ, ψ which satisfy Helmholtz equations with complex propagation constants as follows

$$(\nabla_{r\theta}^2 + \kappa_d^2)\phi = 0, \quad (\nabla_{r\theta}^2 + \kappa_s^2)\psi = 0. \tag{6}$$

The (complex) wavenumber κ_s was defined in eqn (5) and analogously, we define

$$\kappa_d^2 = \omega^2/[c_d^2(1 - i\omega M)], \quad M = (\lambda_v + 2\mu_v)/(\lambda_e + 2\mu_e) \tag{7}$$

to be the (complex) wavenumber of dilatational waves. These waves have speed $c_d = \{(\lambda_e + 2\mu_e)/\rho\}^{1/2}$.

All the non-vanishing components of the displacement and the stress fields can be obtained from the two potentials ϕ, ψ and the pertinent relations are as given below. For the displacements:

$$\begin{aligned} u_r &= \frac{\partial}{\partial r}\left[\phi + \frac{\partial}{\partial r}(r\psi)\right] + r\kappa_s^2\psi \\ u_\theta &= \frac{1}{r}\frac{\partial}{\partial \theta}\left[\phi + \frac{\partial}{\partial r}(r\psi)\right] \\ u_\phi &= 0 \end{aligned} \tag{8}$$

and for the stresses:

$$\begin{aligned} \tau_{rr} &= -[\lambda_e - i\omega\lambda_v]\kappa_d^2\phi + 2(\mu_e - i\omega\mu_v)\left\{\frac{\partial^2}{\partial r^2}\left[\phi + \frac{\partial}{\partial r}(r\psi)\right] + \kappa_s^2\frac{\partial}{\partial r}(r\psi)\right\} \\ \tau_{r\theta} &= [\mu_e - i\omega\mu_v]\left\{2\frac{\partial}{\partial r}\left[\frac{1}{r}\frac{\partial}{\partial \theta}\left[\phi + \frac{\partial}{\partial r}(r\psi)\right]\right] + \kappa_s^2\frac{\partial \psi}{\partial \theta}\right\} \\ \tau_{\theta\theta} &= -[\lambda_e - i\omega\lambda_v]\kappa_d^2\phi + 2(\mu_e - i\omega\mu_v)\left[\left[\frac{1}{r}\frac{\partial}{\partial r} + \frac{1}{r^2}\frac{\partial^2}{\partial \theta^2}\right]\left[\phi + \frac{\partial}{\partial r}(r\psi)\right] + \kappa_s^2\psi\right] \\ \tau_{\phi\phi} &= -[\lambda_e - i\omega\lambda_v]\kappa_d^2\phi + 2(\mu_e - i\omega\mu_v)\left\{\left[\frac{1}{r}\frac{\partial}{\partial r} + \frac{\cot\theta}{r^2}\frac{\partial}{\partial \theta}\right]\left[\phi + \frac{\partial}{\partial r}(r\psi)\right] + \kappa_s^2\psi\right\}. \end{aligned} \tag{9}$$

The procedure to solve the coupled eqns (2) is to solve eqns (6) subject to suitable (stress or displacement) boundary conditions making use of eqns (9) and (8) and then construct the displacement fields from the potentials by means of eqns (8). Anticipating results of the following section we can state that the boundary conditions imposed on the three interfaces of the boundary value problem to be solved next, will determine the ten sets of constants appearing in the general solutions.

2. NORMAL-MODE SOLUTION IN ALL LAYERS

An elastic spherical shell of inner and outer radius a and b respectively is coated with an absorbing layer of outer radius c. This absorbing layer is ideally bonded to the elastic metal shell. The shell contains air in its interior and the whole structure is immersed in water. The Kelvin–Voigt modkl controls the viscoelastic behavior of the coating layer. This layer is the only one that absorbs sound energy. A plane acoustic wave is incident on the coated shell from its South pole, and it is scattered by it. We wish to determine the scattering cross-section of the structure particularly in the backscattering direction $\theta = \pi$. We also want to quantitatively determine the effect produced on the object's sonar cross-section by various amounts of viscous losses present in the coating layer. The four media in question are: (1) the water, (2) the viscoelastic coating, (3) the metal shell, and (4) the interior air. (See Fig. 1).

The pressure wave incident of the structure's South pole is

$$p_{inc} = p_0 e^{-i\omega t} \sum_{n=0}^{\infty} i^n (2n+1) P_n(\cos\theta) j_n(k_1 r) = p_0 e^{i(k_1 r\cos\theta - \omega t)} \tag{10}$$

where $k_1 = \omega/c_1$ and c_1 is the sound speed in water. Since this problem has no azimuthal dependence, the total pressure field in the exterior medium (1) is:

$$p_1 = p_0 e^{-i\omega t} \sum_{n=0}^{\infty} i^n (2n+1) P_n(\cos\theta)[j_n(k_1 r) + b_n h_n^{(1)}(k_1 r)] \tag{11}$$

where spherical Hankel functions of the first kind are chosen to have outgoing scattered waves from the structure and b_n is a coefficient to be determined from the boundary conditions. Displacements associated with this pressure field are found by the relation

$$u_r^{(1)} = \frac{1}{\rho_1 \omega^2} \frac{\partial p_1}{\partial r} \tag{12}$$

where ρ_1 is the density of the exterior fluid. The two scalar potentials ϕ_2, ψ_2 in the viscoelastic coating (i.e. medium (2)) which satisfy eqns (6) are

$$\phi_2(r, \theta, t) = p_0 e^{-i\omega t} \sum_{n=0}^{\infty} i^n (2n+1) P_n(\cos\theta)[c_n j_n(\kappa_{d_2} r) + d_n y_n(\kappa_{d_2} r)]$$

$$\psi_2(r, \theta, t) = p_0 e^{-i\omega t} \sum_{n=0}^{\infty} i^n (2n+1) P_n(\cos\theta)[e_n j_n(\kappa_{s_2} r) + f_n y_n(\kappa_{s_2} r).] \tag{13}$$

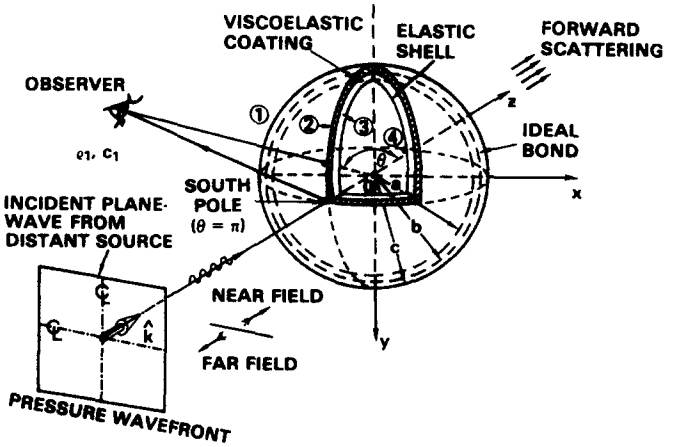

Fig. 1. The geometry of the structure and the incident waveform. Spherical air-filled, steel shell, coated with a rubber layer, immersed in water and insonified by a plane pressure wave incident on its South pole ($\theta = \pi$).

The displacement and stress components associated with these potentials can be found in medium (2) by means of eqns (8) and (9) respectively. The elastic solutions in the spherical shell are found in a way analogous to eqns (13), and the result is,

$$\phi_3(r,\theta,t) = p_0 e^{-i\omega t} \sum_{n=0}^{\infty} i^n(2n+1)P_n(\cos\theta)[g_n j_n(k_{d_3}r) + h_n y_n(k_{d_3}r)]$$

$$\psi_3(r,\theta,t) = p_0 e^{-i\omega t} \sum_{n=0}^{\infty} i^n(2n+1)P_n(\cos\theta)[l_n j_n(k_{s_3}r) + m_n y_n(k_{s_3}r)] \tag{14}$$

where the wavenumbers $k_{d_3} = \omega/c_{d_3}$, and $k_{s_3} = \omega/c_{s_3}$ are now real numbers. The displacement and stress components in medium (3) are found from eqns (14) by means of sets of equations analogous to eqns (8) and (9) but with vanishing viscous coefficients, λ_{v_3}, μ_{v_3}. Finally, the solution for the pressure field in the fluid interior to the structure (i.e. medium (4)) is given by

$$p_4(r,\theta,t) = p_0 e^{-i\omega t} \sum_{n=0}^{\infty} i^n(2n+1)P_n(\cos\theta)q_n j_n(k_4 r) \tag{15}$$

where $k_4 = \omega/c_4$, and c_4 is the sound speed in medium (4). Displacements and pressures are related in medium (4) by an equation analogous to eqn (12). We note that all the potentials in the four layers contain a total of ten sets of constants (i.e., b_n, c_n, ... q_n) which must be determined from ten boundary conditions at the interfaces $r = a$, $r = b$, and $r = c$.

The ten boundary conditions are as follows.

At $r = c$,

$$\tau_{rr}^{(2)} = -p_1 \qquad u_r^{(1)} = u_r^{(2)} \qquad \tau_{r\theta}^{(2)} = 0$$

At $r = b$,

$$u_r^{(2)} = u_r^{(3)}, \quad u_\theta^{(2)} = u_\theta^{(3)}, \quad \tau_{rr}^{(2)} = \tau_{rr}^{(3)}, \quad \tau_{r\theta}^{(2)} = \tau_{r\theta}^{(3)} \tag{16}$$

At $r = a$,

$$\tau_{rr}^{(3)} = -p_{4s}, \qquad u_r^{(3)} = u_r^{(4)}, \qquad \tau_{r\theta}^{(3)} = 0.$$

Equations (8) and (9) or their non-viscous counterparts, are to be used in these boundary conditions together with the solutions in eqns (11)–(15). The boundary conditions are merely statements of continuity of stresses and/or displacements across the three interfaces, and they produce a set of ten equations in the ten unknown coefficients as follows

$$\begin{bmatrix} d_{11} & d_{12} & d_{13} & d_{14} & d_{15} & 0 & 0 & 0 & 0 & 0 \\ d_{21} & d_{22} & d_{23} & d_{24} & d_{25} & 0 & 0 & 0 & 0 & 0 \\ 0 & d_{32} & d_{33} & d_{34} & d_{35} & 0 & 0 & 0 & 0 & 0 \\ 0 & d_{42} & d_{43} & d_{44} & d_{45} & d_{46} & d_{47} & d_{48} & d_{49} & 0 \\ 0 & d_{52} & d_{53} & d_{54} & d_{55} & d_{56} & d_{57} & d_{58} & d_{59} & 0 \\ 0 & d_{62} & d_{63} & d_{64} & d_{65} & d_{66} & d_{67} & d_{68} & d_{69} & 0 \\ 0 & d_{72} & d_{73} & d_{74} & d_{75} & d_{76} & d_{77} & d_{78} & d_{79} & 0 \\ 0 & 0 & 0 & 0 & 0 & d_{86} & d_{87} & d_{88} & d_{89} & d_{8,10} \\ 0 & 0 & 0 & 0 & 0 & d_{96} & d_{97} & d_{98} & d_{99} & d_{9,10} \\ 0 & 0 & 0 & 0 & 0 & d_{10,6} & d_{10,7} & d_{10,8} & d_{10,9} & 0 \end{bmatrix} \begin{bmatrix} b_n \\ c_n \\ d_n \\ e_n \\ f_n \\ g_n \\ h_n \\ l_n \\ m_n \\ q_n \end{bmatrix} = \begin{bmatrix} A_1^\dagger \\ A_2^\dagger \\ 0 \\ 0 \\ 0 \\ 0 \\ 0 \\ 0 \\ 0 \\ 0 \end{bmatrix} \tag{17}$$

The sixty non-vanishing coefficients d_{ij} and $A_1^\dagger$, $A_2^\dagger$ are all listed in Appendix A, after a non-dimensionalization procedure discussed elsewhere[23] has been applied to render dimensionless the 10×10 determinant of the matrix D. Any of the unknown coefficients can then be

obtained by means of Cramer's rule. If $|B_n|$ is the determinant which results when the first column of the 10×10 determinant of the matrix D in eqn (17) is replaced by the column vector in the right side of eqn (17), then coefficient b_n is

$$b_n = |B_n|/|D_n|, \tag{18}$$

and the analogously with all the others.

3. THE DIFFERENTIAL AND SONAR SCATTERING CROSS SECTIONS

The differential scattering cross-section in this azimuthally symmetric situation is defined as

$$\frac{d\sigma}{d\Omega} = \frac{d\sigma}{d\theta} = \lim_{r\to\infty}\left[r^2\left|\frac{p_{sc}}{p_{inc}}\right|^2\right]. \tag{19}$$

Using the incident and scattered pressure fields given in eqn (11) and then using the far-filed asymptotic expansion

$$h_n^{(1)}(k_1 r) \underset{r\gg 1}{\longrightarrow} \frac{(-1)^n}{ik_1 r} e^{ik_1 r}, \tag{20}$$

yields eventually

$$\frac{d\sigma}{d\theta} = \frac{1}{k_1^2}\left|\sum_{n=0}^{\infty}(2n+1)b_n P_n(\cos\theta)\right|^2, \tag{21}$$

which is the differential scattering cross-section, which only depends on *one* of the ten coefficients (viz, b_n).

The sonar cross-section of monostatic (i.e. $\theta = \pi$) sonars is,

$$\sigma \equiv 4\pi\left[\frac{d\sigma}{d\theta}\right]_{\theta=\pi} = \frac{4\pi}{k_1^2}\left|\sum_{n=0}^{\infty}(-1)^n b_n(2n+1)\right|^2 \tag{22}$$

where we have used the relation $P_n(-1) = (-1)^n$. The backscattering cross-section σ is denoted the "sonar" cross-section since it displays the features and levels used by a distant sonar system to "see" the coated structure discussed here. Eqs. (21) and (22) can be made non-dimensional as follows:

$$\frac{4}{c^2}\frac{d\sigma}{d\theta} = \left|\frac{2}{ik_1 c}\sum_{N=0}^{\infty}(2n+1)b_n P_n(\cos\theta)\right|^2 = |f(\theta)|^2, \tag{23}$$

$$\frac{\sigma}{\pi c^2} = \left|\frac{2}{ik_1 c}\sum_{n=0}^{\infty}(-1)^n b_n(2n+1)\right|^2 = |f(\pi)|^2. \tag{24}$$

Series of this type are slowly convergent, and many terms are needed to plot them in wide $k_1 c$-ranges. For $k_1 c \leq 20$, plots of the above equations can be produced without great computational difficulty.

The following numerical values were used for the materials and the geometry. The radii are: $a = 25.40$ cm, $b = 26.3525$ cm, and $c = 26.67$ cm. This corresponds to a 1/8 in coating on a 3/8 in shell having a 10 in. inner radius. Medium (1) is water of parameters $\rho_1 = 1.0\,\text{g/cm}^3$, $c_1 = 1.5 \times 10^5$ cm/sec, and $k_1 = \omega/c_1$. Medium (2) is rubber of parameter $\rho_2 = 1.13\,\text{g/cm}^3$, $\lambda_{e_2} = 2.218 \times 10^{10}\,\text{dyn/cm}^2$, $\mu_{e_2} = 1.0 \times 10^8\,\text{dyn/cm}^2$, and $\lambda_{v_2} = F/\omega$, $\mu_{v_2} = F\dagger/\omega$. The quantities F and $F\dagger$ are numerically varied over suitable ranges discussed below. The speed of dilatational and of shear waves are found by the relations

$$c_{d_2} = [(\lambda_{e_2} + 2\mu_{e_2})/\rho]^{1/2}, \quad c_{s_2} = [\mu_{e_2}/\rho_2]^{1/2}, \tag{25}$$

and they are $c_{d_2} \approx 1.4 \times 10^5$ cm/sec and $c_{s_2} \cong 0.94 \times 10^4$ cm/sec. The (complex) propagation

constants for dilatational and shear waves in medium (2) multiplied times the outer coating radius c can be expressed in terms of the propagation constant of the outer medium k_1 as follows

$$\kappa_{d_2}c = \frac{c_1}{c_{d_2}}\frac{k_1 c}{\sqrt{1 - i[(F + 2F\dagger)/\rho_2 c_{d_2}^2]}}, \quad \kappa_{s_2}c = \frac{c_1}{c_{s_2}}\frac{k_1 c}{\sqrt{1 - i(F\dagger/\rho_2 c_{s_2}^2)}}. \tag{26}$$

Medium (3) is steel of parameters $\rho_3 = 7.84\,\text{g/cm}^3$, $\lambda_{e_3} = 11.3 \times 10^{11}\,\text{dyn/cm}^2$, $\mu_{e_3} = 7.54 \times 10^{11}\,\text{dyn/cm}^2$, and $k_{d_3} = \omega/c_{d_3}$ and k_{s_3} and $k_{s_3} = \omega/c_{s_3}$. The wavespeeds c_{d_3}, c_{s_3} are determined from relations analogous to eqns (25). Medium (4) is air at 20°C of parameters $\rho_4 = 0.0012\,\text{g/cm}^3$, $c_4 = 0.344 \times 10^5\,\text{cm/sec}$ and $k_4 = \omega/c_4$. Levels of viscosity in the coating (i.e. medium (1)) are achieved by numerically varying the parameters F and $F\dagger$ as follows:

Table 1.

	Basic	8b)	8d) = 7a)	7c)
F	0	8.752×10^8	1.243×10^8	1.283×10^8
$F\dagger$	0	10^7	10^7	6×10^6

The labels 8b), 8d), etc... correspond to those in Table 2 of Ref. [30].

4. ISOLATION OF THE MODAL RE-RADIATING COMPONENTS.

Each modal contribution ($n = 0, 1, 2, \ldots$) such as those in Fig. 3, adding up to the cross-section in Fig. 2, can be split into two components. That was one of the earliest findings of the body of knowledge now called the "Resonance Scattering Theory" [30–32]. The two components are a smooth background or shape factor, which accounts for the reflection from the structure as if it were impenetrable (i.e. without interior fields) and another component due to the interior structural resonances of the bilaminar shell, which causes it to re-radiate sound energy. Therefore, acoustic fields penetrate into the structure only through a countable discrete set of narrow spectral windows centered at the natural frequencies of the coated target. Away from these resonances, the acoustic behavior of the structure is as if it were perfectly impenetrable. Thus, the masking effect of the coating will manifest itself by affecting only the re-radiating resonance components of each modal contribution to the shells's sonar cross-section. The modal backgrounds, which depend on the shell shape, will not be altered by the presence of the coating layer in any way. In what follows we will show how this decomposition into shape-factors and re-radiating resonances is achieved in this case. We introduce the definition of the scattering coefficient S_n as follows

$$S_n = 1 + 2b_n. \tag{27}$$

This is merely a particular case of the matrix equation relating the S and T matrices [33]. It is now possible to write the coefficient b_n given in eqn (18) by expanding the determinants $|B_n|$ and $|D_n|$ along their first columns, as follows

$$b_n = \frac{1}{2}(S_n - 1) = \frac{A\dagger D_n^{11} - A_2^* D_n^{21}}{d_{11} D_n^{11} - d_{21} D_n^{21}} \tag{28}$$

where D_n^{11} and D_n^{21} are the minor determinants of the elements d_{11} and d_{21}, shown in eqn (17), and listed in Appendix A. Substituting the values of $A\dagger$, A_2^*, d_{11}, and d_{21} from Appendix A yields,

$$S_n = -\frac{\frac{\rho_1}{\rho_2}\kappa_{s_2}^2 c^2 h_n^{(2)}(k_1 c) D_n^{11} + k_1 c h_n^{(2)\prime}(k_1 c) D_n^{21}}{\frac{\rho_1}{\rho_2}\kappa_{s_2}^2 c^2 h_n^{(1)}(k_1 c) D_n^{11} + k_1 c h_n^{(1)\prime}(k_1 c) D_n^{21}}. \tag{29}$$

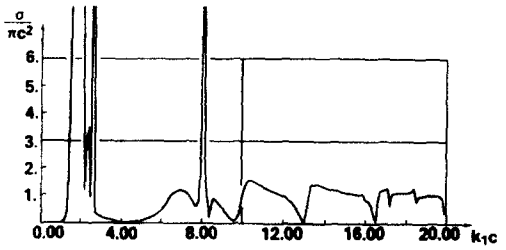

Fig. 2. Normalized (summed) backscattering cross section ($\sigma/\pi c^2 = |\Sigma_n f_n(\pi)|^2$) of a coated, air-filled, steel spherical shell of outer radius c, in water, versus non-dimensional frequency k_1c. Thirty partial waves ($n = 0, 1, 2 \ldots$) are added to generate this plot. Some of the observed "resonance features" in this graph originate from the shell while some others are caused by the coating layer.

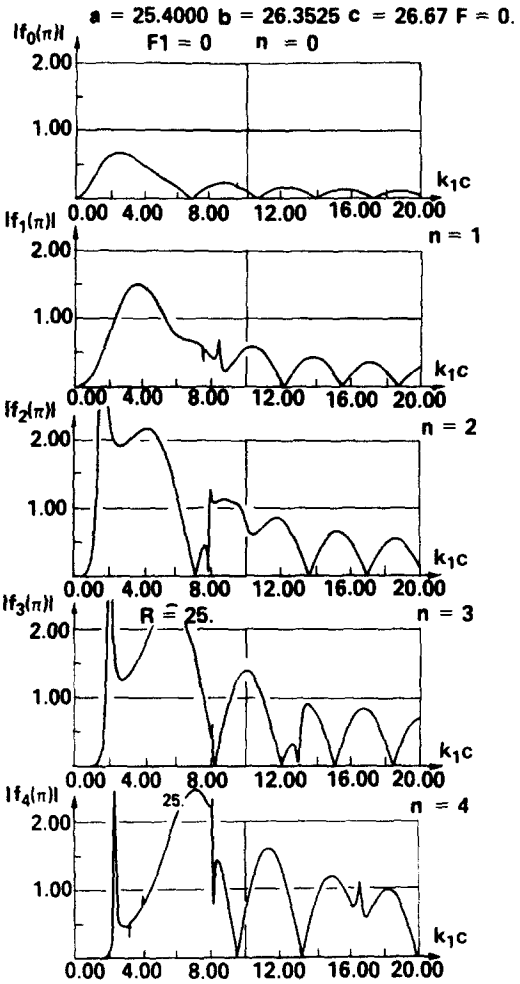

Fig. 3. Plots of the first five ($n = 0, 1, 2, 3, \& 4$) normal modes or partial waves which add up to the summed backscattering (i.e. sonar) cross section displayed in Fig. 2 for a rubber coated, air-filled, spherical steel shell in water, all versus $k_1c (0 \le k_1c \le 20)$.

We can now write S_n in two alternative forms, depending on how we factor the terms in eqn (29). These two forms are

$$S_n = S_n^{(s)} \cdot \frac{z_2 - F_n}{z_1 - F_n} \equiv e^{2i\delta_n} \tag{30}$$

and

$$S_n = S_n^{(r)} \frac{z_2^{-1} - F_n^{-1}}{z_1^{-1} - F_n^{-1}} \equiv e^{2i\delta_n} \tag{31}$$

where,

$$S_n^{(s)} = -\frac{h_n^{(2)}(k_1c)}{h_n^{(1)}(k_1c)} \equiv e^{2i\xi_n^{(s)}} = [S_n]_{\rho_2=0} \tag{32a}$$

$$S_n^{(r)} = -\frac{h_n^{(2)'}(k_1c)}{h_n^{(1)'}(k_1c)} \equiv e^{2i\xi_n^{(r)}} = [S_n]_{\rho_1=0} \tag{32b}$$

$$F_n = -\frac{\rho_1}{\rho_2}\kappa_{s_2}^2 c^2 \cdot \frac{D_n^{11}}{D_n^{21}} \tag{33}$$

and

$$z_i = \frac{k_1 c h_n^{(i)'}(k_1c)}{h_n^{(i)}(k_1c)} \quad (i = 1, 2). \tag{34}$$

From eqn (30) it is clear that if $\rho_1 \gg \rho_2$ (i.e. a "soft" target compared to the ambient medium) then, $F_n \gg 1$ and $S_n \to S_n^{(s)}$. From eqn (31) if $\rho_1 \ll \rho_2$ (i.e. a "rigid" target much denser than the ambient medium) then, $F_n \ll 1$ and $S_n \to S_n^{(r)}$. Note that three phase angles δ_n, $\xi_n^{(s)}$, $\xi_n^{(r)}$, have been defined above, by eqns (30)–(32).

An immediate consequence of the above limiting results is that if a structure with many layers is covered by another layer, no matter how thin, of nearly zero (or nearly infinite) density material compared to that of the outer medium, the echo from the entire structure will be almost identical to that returned from a perfectly soft (or rigid) surface, regardless of which other materials or internal structural components are contained inside that very tenuous (or very dense) outer layer. The above follows immediately because only the density of that outer layer (i.e. ρ_2) has to be compared to the ambient density (i.e. ρ_1) for the above limiting results to be valid. In fact, this is what we have proved in the immediately preceeding paragraph.

The quantities $S_n^{(s)}$ and $S_n^{(r)}$ are the "backgrounds" associated with the shape of the structure, the z_i (and z_i^{-1}) $(i = 1, 2)$ are proportional to the modal *acoustic* impedances of the shell, while F_n (or F_n^{-1}) are proportional to its modal *mechanical* impedance in either the soft or rigid situations, respectively[34]. The "resonances" causing re-radiation are given by the zeroes of the denominators of eqns (30) and (31), which in each case lead to the characteristic equations

$$z_1(x_{nl}^{(s)}) = F_n(x_{nl}^{(s)}) \text{ or } z_1^{-1}(x_{nl}^{(r)}) = F_n^{-1}(x_{nl}^{(r)}) \tag{35}$$

where $x \equiv k_1 c$. To solve these equations is no simple task since each of the 9×9 determinants D_n^{11}, D_n^{21} contains 54 non-vanishing elements, all containing numerous spherical Bessel and Hankel functions (of possibly complex arguments.) The solutions will be the complex eigenfrequencies of the problem, but since it is more convenient to deal with real resonance frequencies, we solve instead

$$\text{Re } z_1(x_{nl}^{(s)}) - F_n(x_{nl}^{(s)}) = 0 \text{ and } \text{Re } z_1^{-1}(x_{nl}^{(r)}) - F_n^{-1}(x_{nl}^{(r)}) = 0 \tag{36}$$

for the soft and rigid situations, respectively.

Simple algebraic manipulations suffice to show that the definition $S_n \equiv \exp[2i\delta_n]$ implies that

$$S_n - 1 = 2i \sin \delta_n \exp(i\delta_n), \tag{37}$$

that eqn (30) implies that

$$S_n - 1 = e^{2i\xi_n^{(s)}}\left[\frac{z_2 - z_1}{z_1 - F_n} + 2i\, e^{-i\xi_n^{(s)}} \sin \xi_n^{(s)}\right], \tag{38a}$$

and that eqn (31) implies that

$$S_n - 1 = e^{2i\xi_n^{(r)}}\left[\frac{z_2^{-1} - z_1^{-1}}{z_1^{-1} - F_n^{-1}} + 2ie^{-i\xi_n^{(r)}} \sin \xi_n^{(r)}\right]. \tag{38b}$$

The magnitudes of the scattering amplitudes given in eqn (24), which we repeat here in a more complete form

$$\frac{\sigma}{\pi c^2} = |f(\pi)|^2 = \left|\sum_{n=0}^{\infty} f_n(\pi)\right|^2 = \left|\frac{2}{ix}\sum (-1)^n(2n+1)b_n\right|^2$$

are, therefore,

$$|f_n(\pi)| = \left|\frac{2n+1}{x}(S_n - 1)\right| = \left|\frac{2n+1}{x} e^{2i\xi_n^{(s)}}\left[\frac{z_1 - z_2}{F_n - \mathrm{Re}\, z_1 - i\,\mathrm{Im}\, z_1} + 2i\, e^{-i\xi_n^{(s)}} \sin \xi_n^{(s)}\right]\right| \tag{39a}$$

for the soft case, and analogously

$$|f_n(\pi)| = \left|\frac{2n+1}{x} e^{2i\xi_n^{(r)}}\left[\frac{z_1^{-1} - z_2^{-1}}{F_n^{-1} - \mathrm{Re}\, z_1^{-1} - i\,\mathrm{Im}\, z_1^{-1}} + 2i\, e^{-i\xi_n^{(r)}} \sin \xi_n^{(r)}\right]\right| \tag{39b}$$

for the rigid case. These are the partial waves ($n = 0, 1, 2$ and 3) displayed in Fig. 3. Equations (39) are still exact and they can still be linearized in the now standard way of the Resonance Scattering Theory[31], however, that will not be shown here. The exact form of eqns (39) already shows how each partial wave contains two components, one associated with the structural *resonances* that cause re-radiation, represented by the fraction in eqns (39), and the other the *shape factor* or background, associated with reflection from an impenetrable structure represented by the term with the sine functions. We note the following two valid relationships

$$S_n^{(s)} - 1 = 2i\, e^{i\xi_n^{(s)}} \sin \xi_n^{(s)} \tag{40a}$$

$$S_n^{(r)} - 1 = 2i\, e^{i\xi_n^{(r)}} \sin \xi_n^{(r)}. \tag{40b}$$

Therefore, in the soft and rigid cases respectively, the contributions from each of the shape factors to the scattering amplitudes are

$$|f_n^{(s)s.f.}(\pi)| = \left|\frac{2n+1}{x} 2i\, e^{i\xi_n^{(s)}} \sin \xi_n^{(s)}\right| \tag{41a}$$

$$|f_n^{(r)s.f.}(\pi)| = \left|\frac{2n+1}{x} 2 \sin \xi_n^{(r)}\right|. \tag{41b}$$

Analogously, the corresponding contributions from the re-radiating resonances are

$$|f_n^{(s)res}(\pi)| = \left|\frac{2n+1}{x} e^{2i\xi_n^{(s)}} \frac{z_1 - z_2}{F_n - z_1}\right| = \left|\frac{2n+1}{x}[2b_n - (S_n^{(s)} - 1)]\right| \tag{42a}$$

$$|f_n^{(r)res}(\pi)| = \left|\frac{2n+1}{x} e^{2i\xi_n^{(r)}} \frac{z_1^{-1} - z_2^{-1}}{F_n^{-1} - z_1^{-1}}\right| = \left|\frac{2n+1}{x}[2b_n - (S_n^{(r)} - 1)]\right|. \tag{42b}$$

These components will be plotted separatedly in the next section. We note that both eqns (41) or both eqns (42) represent the same result that has been split up into two components in two different ways. Equations (41a) and (42a) represent the split in the soft case, while eqns (41b) and (42b) in the rigid case.

A third and final situation requiring analysis occurs when the shape factor that should be subtracted from the modal scattering coefficients in order to isolate the resonances is neither rigid nor soft but somewhere in between these two extremes[31]. From eqns (27), (30) and (31) it follows that the proper coefficients to use in the soft and rigid cases, respectively, are

$$2(b_n - b_n^{(s)}) = S_n - S_n^{(s)} = S_n^{(s)} \frac{z_1 - z_2}{F_n - z_1}, \tag{45a}$$

$$2(b_n - b_n^{(r)}) = S_n - S_n^{(r)} = S_n^{(r)} \frac{z_1^{-1} - z_2^{-1}}{F_n^{-1} - z_1^{-1}}. \tag{45b}$$

These are the quantities we have used in eqns (42) to construct their contributions to the scattering amplitudes. It is simple to verify that for the situation somewhere midway between the above two cases, the analogous result to be used is

$$2(b_n - b_n^{(m)}) = S_n - S_n^{(m)} = S_n^{(m)} \cdot \frac{\bar{z}_1^{-1} - \bar{z}_2^{-1}}{\bar{F}_n^{-1} - \bar{z}_1^{-1}}, \tag{46}$$

where the quantities with bars are defined to be

$$\begin{aligned} \bar{z}_i(x) &= z_i(x) - F_n(x_0)\,(i = 1, 2) \\ \bar{F}_n(x) &= F_n(x) - F_n(x_0), \end{aligned} \tag{47}$$

and the midway shape-factor $S_n^{(m)}$ is defined to be

$$S_n^{(m)} \equiv S_n^{(s)} \frac{\bar{z}_2}{\bar{z}_1} = S_n^{(s)} \frac{z_2 - F_n(x_0)}{z_1 - F_n(x_0)} \equiv e^{2i(\xi_n^{(s)} - \alpha)}, \tag{48}$$

which is clearly unitary since it is quickly verified that

$$\alpha = \arg(z_1 - F_n(x_0)) = -\arg(z_2 - F_n(x_0)). \tag{49}$$

The explicit expression for S_n in terms of the midway shape factor $S_n^{(m)}$ is

$$S_n = S_n^{(m)} \frac{\bar{z}_2^{-1} - \bar{F}_n^{-1}}{\bar{z}_1^{-1} - \bar{F}_n^{-1}}, \tag{50}$$

which is analogous to eqns (30) and (31) for the rigid and soft cases. The quantities F_n, z_1, and z_2 are given in eqns (33) and (34). and x_0 is a value of x for which $F_n(x_0)$ is nearly constant. Plots of $F_n(x)$ vs x show that in most cases this function is nearly constant almost everywhere except near its singularities which are close to the resonances of the coated shell [which are found as the roots of the real parts of the denominators of eqns (46) or (50)] due to the usual smallness of the quantity $\mathrm{Re}\,(\bar{z}_1)^{-1}$. The choice of x_0 is *not* critical, and the counterpart of eqn (42) in this midway case is

$$|f_n^{(m)res}(\pi)| = \left| \frac{2n+1}{x} e^{2i(\xi_n^{(s)} - \alpha)} \frac{\bar{z}_1^{-1} - \bar{z}_2^{-1}}{\bar{F}_n^{-1} - \bar{z}_1^{-1}} \right| = \left| \frac{2n+1}{x} [2b_n - (S_n^{(m)} - 1)] \right|. \tag{51}$$

5. NUMERICAL RESULTS.

The first objective of this paper was to display the computed *back*scattering (i.e. sonar) cross section of the coated shell as given by eqn (24) with b_n given in eqn (18), as a function of the acoustical size of the structure $k_1 c$, in the outer medium. Later we analyze the effect the three viscous levels shown in Table 1 have on the above described spectral plot of the cross section. The computations required to generate these graphs make use of routines we generated years ago to evaluate spherical (and also standard) Bessel, Neumann and Hankel functions of complex arguments and fractional (or integer) orders. The analysis is arbitrarily done for a coated shell with an outer radius $c = 26.67$ cm and $k_1 c$ varying up to a value of 20. This means that the frequencies of the incident waves range from zero to about 18 kHz, which is a band covering many cases of interest.

Figure 2 displays the plot of eqn (24) versus $k_1 c$ ($0 \le k_1 c \le 20$) assuming that the rubber in medium (2) is elastic, but nonabsorbing. Twenty-five terms were kept in the sum used to generate Fig. 2 to insure accuracy in the $k_1 c$-range considered there. Since the plot is the sum of many (i.e. 25) partial-waves or normal modes, which interfere one with the next in a sensitive

fashion, the plot exhibits many rapid oscillations, peaks, and deep minima which are ultimately due to resonances excited in the shell and/or coating layers by the incident wave.

We will later show how the many oscillations present in Fig. 2 are damped out as the viscous levels of the coating layer increase through the values shown in Table 1. The first five partial waves that add-up to the cross section in Fig. 2 are displayed in Fig. 3 for $n = 0, 1, \ldots 4$, from top to bottom. These waves are the spectra of the modal contributions contained within eqn (24), viz.

$$|f_n(\pi)| = \left|\frac{2}{ik_1c}(-1)^n(2n+1)b_n\right| \tag{52}$$

versus k_1c, where b_n, given in eqn (18) depends on the k_1c in a complicated fashion, as it is evident from inspection of the list of elements d_{ij} in Appendix A. We further note that the *square* of the sum of the modal amplitudes defines the (normalized) cross section given in eqn (24), viz.

$$\left|\sum_{n=0}^{\infty} f_n(\pi)\right|^2 = |f(\pi)|^2 = \sigma/\pi c^2. \tag{53}$$

Each rapid oscillation appearing in Fig. 2 is caused by resonances present in these normal-mode contributions shown in Fig. 3. Note for example the one near $k_1c \approx 8$ in the plots of various modes (i.e. $n = 1, 2, 3, 4, \ldots$) which consequently manifests itself as a very large spike in Fig. 2. Note that in view of eqn (53) the ordinates in Fig. 2 are the squares of those in Fig. 3. Observation of Fig. 2 show regions (around $k_1c \approx 2$ and 8) where the cross sectional values are at least six times larger than those predicted by geometrical acoustics (i.e. πc^2). These are frequency bands at which the target is highly "visible" in spite of the presence of the outer absorbing layer. One reason for this result is that for the plots shown in Figs. 2 and 3, the coating layer was assumed non-absorbing, and therefore, completely incapable of reducing the backscattered return. The absorptive behavior of the coating is investigated in later figures.

The quantitative effect of coating viscosity on the (summed) cross section shown in Fig. 2 without viscous effects, is now shown in Fig. 4. The three shown viscous levels correspond to the three (non-vanishing) sets of values in Table 1. These viscous parameters F, $F^{\dagger}$ make the arguments of the Bessel functions in the coating layer (viz. $\kappa_{d_2}c$, $\kappa_{s_2}c$) take on complex values related to k_1c through eqns (26). As the absorption levels increase, certain resonance features of the cross section begin to get damped out. Note for example the large spike near $k_1c \approx 8$ in Fig. 2. In the top portion of Fig. 4, that spike is much reduced, while in the central and bottom parts of Fig. 4, it is totally gone. Note that at these higher viscous levels there are some spikes in the high-frequency end (i.e. for $k_1c \geq 18$) that were not present in Fig. 2. These are caused by numerical instabilities in the subroutines to evaluate Bessel functions of complex arguments with large moduli, and should not be attributed to any type of cross sectional enhancement effect due to the coating at all. Figure 5 shows the quantitative effect of viscous absorption on the first four modes contained within the cross section. As we increase the viscous levels through the values listed in Table 1, we note that some of the resonance features present in the modal plots are damped out and eventually disappear. The modal backgrounds or shape factors to be discussed and subtracted in Fig. 6 (left column) are seen to remain unaffected by increasing absorptive levels. Some of the numerical instabilities mentioned earlier in the discussion of Fig. 4 are also present at the higher viscous levels (right column), particularly at the high-frequency end (i.e. $k_1c \geq 18$) of Fig. 5. Some resonance features clearly visible in the left column, where they have been marked by rectangular boxes, eventually disappear at the higher viscous levels shown in the right column.

The material combinations of the bilaminar shell studied in this paper such that the shell has an overall acoustic behavior close to the rigid. This conclusion emerges from the following analysis of Figs. 6 and 7 where we attempt to isolate the re-radiation or resonance components contained within each mode ($n = 0, 1, 2, \ldots$) by subtracting first the rigid shape factors (Fig. 6, left column), and then the soft ones (Fig. 7, left column) from the modal contributions to the cross section plotted earlier in Fig. 3.

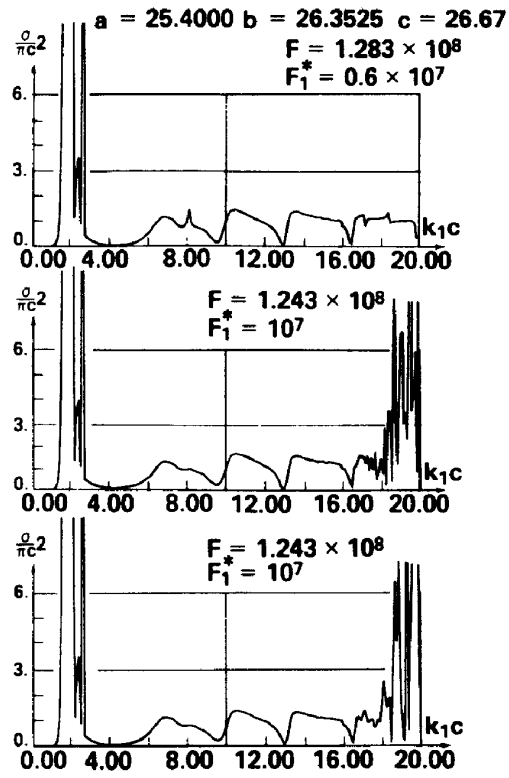

Fig. 4. The quantitative effect of coating absorption on the (summed) sonar cross section. As the absorption levels increase, the amplitudes of the resonance spikes decrease from their original values in Fig. 2, where no absorption was accounted for. For higher absorption and higher frequencies (i.e. $k_1c \geq 18$) numerical instabilities start to develop in the plots.

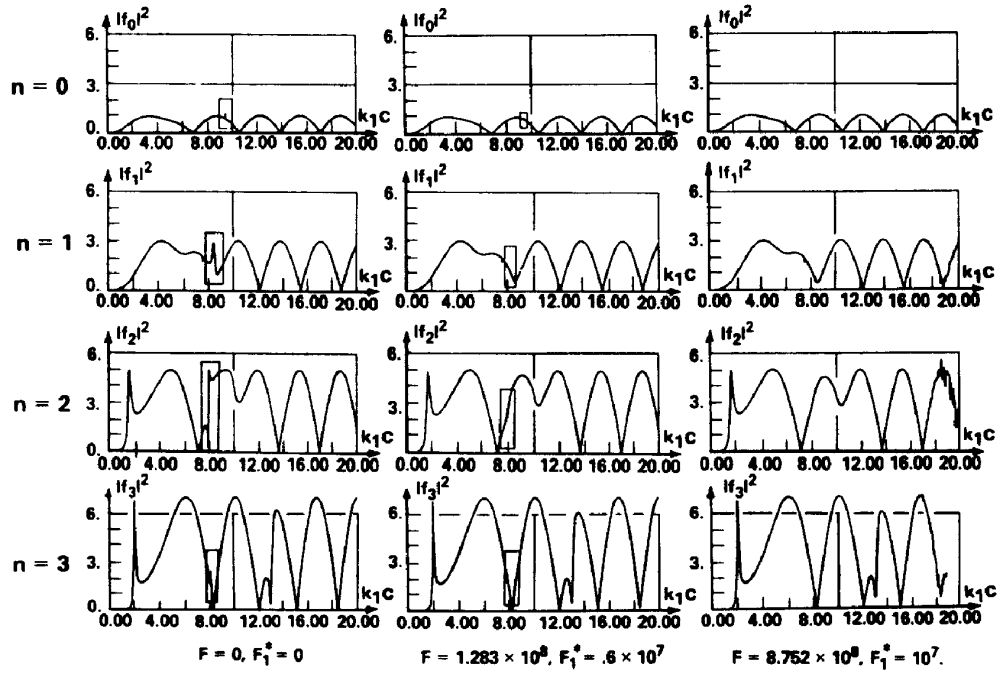

Fig. 5. The quantitative effect of coating absorption on each one of the partial waves ($n = 0, 1, 2, 3$) contained within the summed cross section of Fig. 2. Increasing the coating viscosity (left to right columns) does not alter the "backgrounds" but it damps out certain clearly visible (note boxes) resonances superimposed on them.

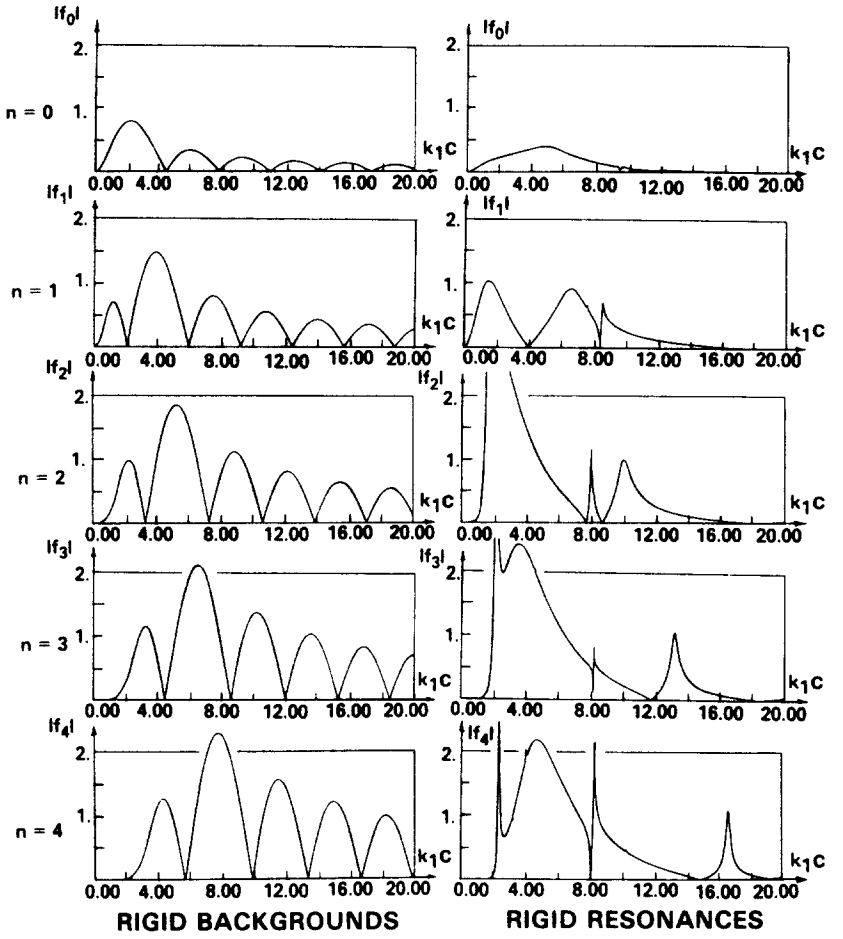

Fig. 6. Extraction of the "rigid resonances" of the bilaminar shell (right column) from the first five (undamped) partial waves displayed earlier in Fig. 3, by subtraction of the corresponding modal "rigid backgrounds" (left column), of a perfectly rigid but otherwise identical spherical structure of dia. 2c. These rigid resonances seem to group themselves into two (broad and narrow) overlapping subfamilies.

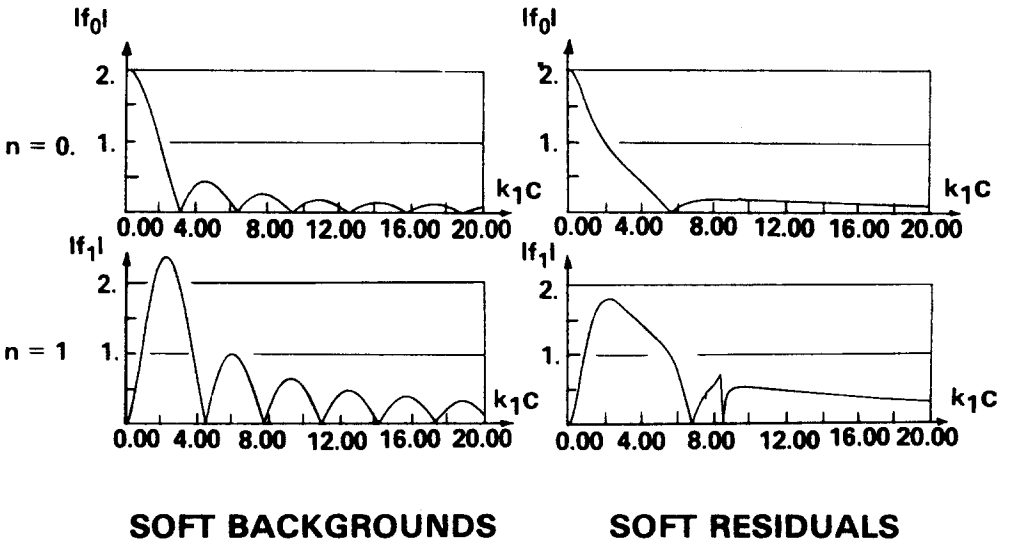

Fig. 7. Subtraction of the modal ($n = 0, 1$) "soft backgrounds" (left column) of a perfectly soft spherical structure of dia. 2c from the modal contributions shown earlier in Fig. 3, to determine the type of residuals that are left over (right column). (These residuals would have been "soft". This is not the case here since the structure in this instance behaves as "rigid", and these residuals are not resonances at all.)

The left column of Fig. 6 displays the modal shape factors in the rigid case, as given by eqn (41b) for the first five ($n = 0, 1, \ldots, 4$) modes. The right column in Fig. 6 displays the rigid re-radiation (or resonance) portions as given by eqn (42b). The resulting modal resonances are seen to group themselves in two overlapping families which are broad and narrow, respectively. These are the resonances of the bilaminar shell under study. Some of these are resonances of the shell and some are of the coating in a way that we will investigate in further detail in the future.

If the soft shape factors derived in eqn (41a) are subtracted from the modal contributions shown in Fig. 3 in an attempt to isolate "soft resonances" in a way analogous to that followed to generate the rigid resonances in Fig. 6, the procedure yields results that do *not* resemble resonances of any kind. The soft shape factors for the first two modes ($n = 0, 1$) are given in the left column of Fig. 7, and after they are subtracted from the corresponding modes in Fig. 3, the resulting residuals are displayed in the right column of Fig. 7. These residuals do not look like resonances, and in fact, they are not resonances at all. One should not feel disappointed because a given structure does not have both rigid and soft resonances. In fact, that is never the case since only one of several possible behaviors can actually occur for a given structure. In the present case, only the rigid resonances have been shown to be the suitable ones. A third, still possible alternative is that the structure has neither one of those two types of resonances. It is for this alternative that we discussed the case of "midway resonances" in the text from eqn (45) on. To test if the structure has this third type of resonances corresponding to a behavior somewhere *between* rigid and soft, we produced Figs. 9 and 10 below.

Figure 8 compares the two extreme cases of shape factors that we have discussed thus far. This background comparison is illustrated by the second (i.e. $n = 2$) normal mode. The soft shape factor is shown in solid lines while the rigid is shown in dashed lines, both versus $k_1c \equiv x$. For any given mode, purely rigid and purely soft backgrounds always appear interlaced, as it is typically shown in this plot for $n = 2$. Intermediate or "midway" shape factors are shifted relative to these two basic and extreme cases, and they appear displaced somewhere between the two. The plots in Fig. 8 are obtained using eqns (41).

The only case remaining to be investigated is that of the midway resonances. The quantity $F_n(x)$ given in eqn (33), which is (inversely) proportional to the modal mechanical impedance of the coated shell, can be plotted versus $k_1c \equiv x$ with the result shown in Fig. 9 for the second ($n = 2$) mode. Away from the three singularities present in the range $0 \leq x \geq 20$ this is a slowly varying (quasi-constant) function, and the methodology of the midway background discussed at the end of Section IV can be applied to it. Inspection of Fig. 9 shows that $F_2(x_0) \approx 2.5$, and using eqn (51), the "midway resonances" of the second ($n = 2$) mode have been plotted in Fig. 10 and they can be generated analogously for any other mode. Comparing the rigid resonances in Fig. 6 ($n = 2$, right column) with Fig. 10 obtained using the midway resonance procedure, we note that the results are quite similar. Minor differences such as a first resonance slightly narrower than

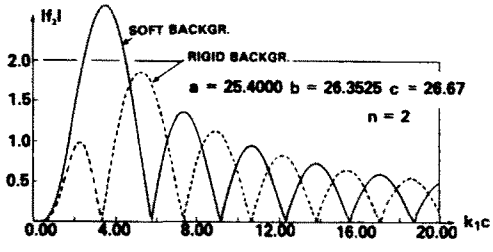

FIGURE 8.

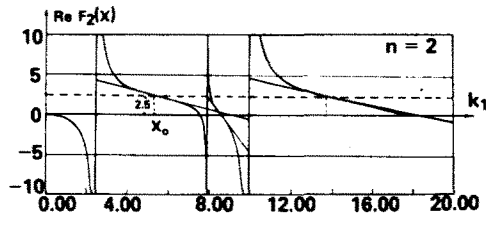

FIGURE 9.

Fig. 8. Comparison of the soft (solid line) and the rigid (dashed) backgrounds for the second ($n = 2$) mode contained within the sonar cross section, as a function of non-dimensional frequency k_1c. For all modes contributing to the cross section, rigid and soft backgrounds are interlaced as typically shown here for the coated, air-filled, spherical, shell in water under analysis.

Fig. 9. Plot of $\mathrm{Re}(F_n)$ vs. $k_1c \equiv x$, where F_n, given in eqn (33), is (inversely) proportional to the modal ($n = 2$) mechanical impedance of the coated shell. Away from its singularities, this function is approximately constant and $F_2(x_0) \cong 2.5$. The calculation is for the same coated, air-filled, spherical, steel shell in water considered here.

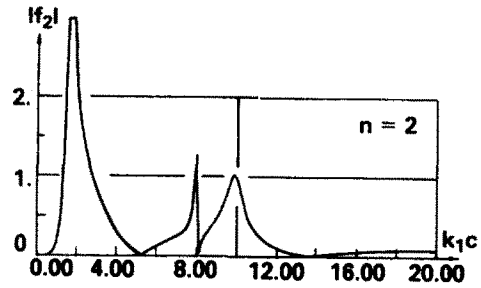

Fig. 10. Graph of the "midway-type" resonances present in the second ($n = 2$) mode versus non-dimensional frequency k_1c, from eqn (51). This graph is very close to the $n = 2$ rigid-resonance case shown in Fig. 6. As obtained by this approach leading to eqn (51), all other modes ($n \neq 2$) contain resonances very close to the rigid resonances displayed in (the right column of) Fig. 6, because for this combination of materials, this coated, fluid-loaded, structure has an overall acoustic behavior relatively close to the rigid.

that shown in Fig. 6 ($n = 2$), are noticeable, but the overall graph is identical to that in Fig. 6 for the second mode as well as for all the others. Various choices of x_0 show that its value is *not* critical. Therefore, the "midway resonance" procedure leading to eqn (51), for the material combination chosen here, produces almost the same resonances isolated earlier in the rigid case (Fig. 6). Thus, the rigid acoustic behavior is the most accurate descriptor of the bilaminar situation under analysis here. If the midway shape factor that yields the midway resonances of the $n = 2$ mode shown in Fig. 10 had been plotted, we would see a graph in-between the rigid and the soft backgrounds shown in Fig. 8 but sufficiently close to the rigid one to further provide the overall quasi-rigid acoustic behavior of this complex shell structure. In other words, the true acoustic behavior of the structure is not sufficiently far away from the rigid "extreme" to merit treatment under the "midway resonance procedure", and thus, this approach reproduces the earlier rigid behavior.

The very realistic situation modelled and analyzed here admits modal shape factors as simple as those associated with the rigid behavior. Subtracting them from the modes, the correct resonances are isolated. We have seen other instances[31] where the *soft* backgrounds are equally suitable for very adequate descriptions of the scattering mechanisms involved. Thus, the neighborhoods near the soft and rigid extremes, where the Resonance Scattering Theory so far has been shown to have most of its usefulness, are in fact quite *wide*. We have shown here another example of the many realistic situations that fit quite well within those neighborhoods. Thus, there is left only a *narrow* gap midway between the two extremes, requiring further study.

6. CONCLUSIONS

We have developed an analytical model to predict the global scattering of acoustic waves from spherical, gas-filled, elastic shells covered with layers of viscoelastic materials. The model is exact insofar as the equations of linear elasticity/viscoelasticity govern the behavior of the submerged bilaminar shell structure. All absorption levels in the outer absorbing layer can be accounted for. Even though this is a coupled problem due to the fluid loading, we have successfuly separated shape factors and re-radiation (i.e. resonance) modal contributions, in the manner of the Resonance Scattering Theory (RST), and we have quantitatively studied some aspects of the damping effects the absorptive layer has on the modal resonances, considering each mode separatedly, or all added together. The particular steel-rubber bilaminar shell used for the displayed calculation has been shown to acoustically behave close to the rigid extreme and this has been further substantiated using the midway-resonance approach also presented here. We emphasize for clarity that there *is* sound penetration into the structure, since it was modelled as an elastic/viscoelastic shell rather than rigid. Had it been purely rigid, each normal mode contained within the cross section would have consisted only of shape factors (or backgrounds) and there would have been no resonances (or re-radiated) portions. The fact that there are appreciable (rigid-type) resonances (Fig. 6 right column) within each mode is a measure of the departure of the structure's acoustic behavior from that of a perfectly impenetrable (rigid) body of the same shape. Our earlier work on RST has shown that sound

penetration into any target takes place only through a countable set of discrete spectral windows centered at the (rigid) resonances of the fluid-loaded structure that we successfuly isolated mode-by-mode in Fig. 6 These peaks are all numerically predicted by the roots $x_{nl}^{(r)}$ of the second one of eqns (35). We envison further work where the exact elasticity/viscoelasticity equations used here, are judiciously replaced by the simpler sets of equations of suitable Shell Theories. The present work will be the standard against which all those approximations will be compared.

Acknowledgements—It is always a pleasure to acknowledge the support and encouragement received from the Naval Surface Weapons Center Independent Research Board (Dr. D. J. Pastine, Director). We further thank John Barlow, also of this Center (K-33), for his assistance in the generation of the computed figures.

REFERENCES

1. M. C. Junger, Sound scattering by thin elastic shells. *J. Acoust. Soc. Amer.* **24**, 366–373 (1952).
2. M. C. Junger, Vibrations of elastic shells in a fluid medium and the associated radiation of sound. *J. Appl. Mech* **14**, 439–445 (1952).
3. M. C. Junger, Normal modes of submerged plates and shells *Fluid-Solid Interaction*, pp. 79–119 (Edited by J. E. Greenspon) ASME Press (1967).
4. A. Kalnins, On the free and forced vibrations of rotationally symmetric layered shells. *J. Appl. Mech.* **32**, 941–943 (1965).
5. A. Kalnins, Dynamic problems of elastic shells. Appl. Mech. Rev. **18**, 867–872 (1965). (Review.)
6. A. H. Shah, C. V. Ramkrishnan and S. K. Datta, Three-dimensional and shell-theory analysis of elastic waves in a hollow sphere. *J. Appl. Mech.* **36**, 431–439 (1969).
7. W. F. Fender, Scattering from an elastic spherical shell. Naval Undersea Center Techn. Rep. NUC-TR-313, San Diego, CA, Oct. 1972.
8. R. Goodman and R. Stern, Reflection and transmission of sound by elastic spherical shells. *J. Acoust. Soc. Amer.* **34**, 338–344 (1962).
9. R. Hickling, Analysis of echoes from a hollow metallic sphere in water. *J. Acoust. Soc. Amer.* **36**, 1124–1137 (1964).
10. K. J. Diercks and R. Hickling, Echoes from hollow aluminium spheres in water. *J. Acoust. Soc. Amer.* **41**, 380–393 (1967).
11. R. Hickling and R. W. Means, Scattering of frequency-modulated pulses by spherical elastic shells in water. *J. Acoust. Soc. Amer.* **44**, 1246–1252 (1968).
12. G. Gaunaurd, Monostatic and Bistatic cross sections of a large sphere partially insonified at a circular spot. *J. Acoust. Soc. Amer.* **61**, 1121–1132 (1977).
13. G. Gaunaurd and H. Überall, Acoustics of finite beams. *J. Acoust. Soc. Amer.* **63**, 5–16 (1978).
14. H. Huang, Transient interaction of plane acoustic waves with a spherical elastic shell. *J. Acoust. Soc. Amer.* **45**, 661–670 (1968).
15. [a]Ye. L. Shenderov, *Wave problems in Hydroacoustics* (1972), Leningrad, U.S.S.R. Translation by: Joint Publications Research Service Report JPRS–58146 (Parts I and II, 433 pp.) of Feb 5 1973, National Technical Information Service, Springfield, VA 22151. [b]Uno K. Nigul, Editor, *Echo Signals from Elastic Objects* (1974) Tallin, Estonian SSR. Translation by: Joint Publications Research Service Report JPRS-63937 (Part *II*) of Jan 22, 1975, National Technical Information Service, Springfield. VA 22151. (262 pp.) *Part I*, Translated by NISC., 4301 Suitland Road, Washington, DC 20390, NISC Translation No. 6271 of March 7, 1980 (472 pp.).
16. P. J. Jackins, High frequency scattering by a sphere with complex surface impedance. Naval Surf. Weap. Center Tech. Rep. TR-81-255, Oct 1981 (in press.) Also Ph, D. Thesis, Catholic University, Washington, DC, 1981.
17. Bruce A. Bolt (Ed., *Methods in Computational Physics* (1972), Vol. *11, Seismology: Surface Waves and Earth Oscillations*, and Vol. *12 Seismology: Body Waves and Sources*, Academic Press, New York.
18. H. E. Morris *et al.*, Interaction of sound with the ocean bottom. Naval Ocean Systems Center Rep. NOSC TR–242, April 30, 1978, San Diego, CA 92152. Also, K. E. Hawker *et al.*, Result of a study of the ocean bottom interacting with underwater sound. Appl. Res. Labs, University of Texas, Austin, TX 78712, Report ARL TR-77-27, 25 Oct. 1977.
19. L. M. Brekhovskikh, *Acoustics of the Ocean*, 1974, Moscow, USSR, Translation by: NISC, 4301 Suitland Road, Washington, DC 20390, NISC Translation No. 4048 of Oct 5, 1978. Chap. 6 and 7. (800 pp.)
20. C. M. Davies, L. Dragonette and L. Flax, Acoustics scattering from silicone rubber cylinders and spheres. *J. Acoust. Soc. Amer.* **63**, 1694–1698 (1978).
21. G. C. Lauchle, Backscattering from absorbent spheres. Penn. State Univ., Applied Res. Lab, Tech. Memo No. TM-79-131, 10 July 1979.
22. R. H. Vogt, L. Flax, L. R. Dragonette and W. G. Neubauer, *Erratum*: Monostatic Reflection of a plane wave from an absorbent sphere. *J. Acoust. Soc. Amer.* **61**, 1315 (1977).
23. G. C. Gaunaurd, Sonar cross section of a coated hollow cylinder in water. *J. Acoust. Soc. Amer.* **61**, 360–368 (1977).
24. L. Flax and W. G. Neubauer, Acoustic reflection from layered elastic absorptive cylinders. *J. Acoust. Soc. Amer.* **61**, 307–312 (1977).
25. G. C. Gaunaurd, High-frequency acoustic scattering from submerged cylindrical shells coated with viscoelastic layers. *J. Acoust. Soc. Amer.* **62**, 503–512 (1977).
26. G. C. Gaunaurd and H. Überall, Numerical evaluation of modal resonances in the echoes of compressional waves scattered from fluid-filled spherical cavities in solids. *J. Appl. Physics* **50** (7), 4642–4659 (1979).
27. J. D. Murphy, J. George, A. Nagl and H. Überall. Isolation of the resonant component in acoustic scattering from fluid-loaded elastic spherical shells. *J. Acoust. Soc. Amer.* **65**, 368–373 (1979).
28. S. Buchan, *Rubber to Metal Bonding*. Crosky/Lockwood, London (1948).
29. G. C. Gaunaurd, Methods for solving the viscoelasticity equations for cylinder and sphere problems. Naval Surface Weapons Center Tech. Rep. NSWC-WOL-76-20, Mar 22, 1976, Silver Spring, MD, 20910 (ADA025–302).

30. G. C. Gaunaurd and H. Überall, Theory of resonant scattering from spherical cavities in elastic and viscoelastic media. *J. Acoust. Soc. Amer.* **63**, 1699–1712. (1978).
31. L. Flax, G. C. Gaunaurd and H. Überall, The Theory of Resonance Scattering. *Physical Acoustics* (Edited by W. P. Mason and R. N. Thurston), Vol. 15, Chap. 3, pp. 191–294. Academic Press, New York (1981). (Review chapter.)
32. G. C. Gaunaurd and H. Überall, Resonances in acoustic and elastic wave-scattering. *Proc. Conf. on: Recent Developments in classical wave-scattering: Focus on the T-Matrix Approach*, pp. 413–430. Pergamon Press Oxford (1980). (Review paper, V. K. Varadan, Editor.)
33. R. G. Newton, *Scattering Theory of Waves and Particles*. McGraw-Hill, New York. (1966). (Eq. 7.58 setting the constant $2\pi i$ equal to -1 in our case.)
34. M. C. Junger and D. Feit, High-frequency response of point-excited submerged spherical shells. *J. Acoust. Soc. Amer.* **45**, 630–636 (1968).

APPENDIX A

The normalized elements of the 10×10 *matrix* D

The normalization procedure followed in this spherical case is identical to that used earlier for a submerged coated cylinder[23]. It turns out that in the same order as they come-out of the boundary conditions, the coefficients of the ten resulting equations have dimensions of (pressure)^4, i.e. (dyn/cm^2)^4. Multiplying certain rows and columns of the resulting determinants by suitable constants, it is possible to non-dimensionalize the sixty non-zero elements. The final result is given below:

$$d_{11} = \frac{\rho_1}{\rho_2}\kappa_{s_2}^2 c^2 h_n^{(1)}(k_1 c)$$

$$d_{12} = -4\kappa_{d_2} c j_n'(\kappa_{d_2} c) + [2n(n+1) - \kappa_{s_2}^2 c^2] j_n(\kappa_{d_2} c)$$

$$d_{13} = -4\kappa_{d_2} c y_n'(\kappa_{d_2} c) + [2n(n+1) - \kappa_{s_2}^2 c^2]\, y_n(\kappa_{d_2} c)$$

$$d_{14} = -2n(n+1)[j_n(\kappa_{s_2} c) - \kappa_{s_2} c j_n'(\kappa_{s_2} c)]$$

$$d_{15} = -2n(n+1)[y_n(\kappa_{s_2} c) - \kappa_{s_2}\, c y_n'(\kappa_{s_2} c)]$$

$$d_{21} = -k_1 c h_n^{(1)'}(k_1 c)$$

$$d_{22} = \kappa_{d_2} c j_n'(\kappa_{d_2} c)$$

$$d_{23} = \kappa_{d_2} c y_n'(\kappa_{d_2} c)$$

$$d_{24} = n(n+1) j_n(\kappa_{s_2} c)$$

$$d_{25} = n(n+1) y_n(\kappa_{s_2} c)$$

$$d_{32} = 2[j_n(\kappa_{d_2} c) - \kappa_{d_2} c j_n'(\kappa_{d_2} c)]$$

$$d_{33} = 2[y_n(\kappa_{d_2} c) - \kappa_{d_2} c y_n'(\kappa_{d_2} c)]$$

$$d_{34} = 2\kappa_{s_2} c j_n'(\kappa_{s_2} c) + [\kappa_{s_2}^2 c^2 - 2n(n+1) + 2] j_n(\kappa_{s_2} c)$$

$$d_{35} = 2\kappa_{s_2} c y_n'(\kappa_{s_2} c) + [\kappa_{s_2}^2 c^2 - 2n(n+1) + 2] y_n(\kappa_{s_2} c)$$

$$d_{42} = \kappa_{d_2} b j_n'(\kappa_{d_2} b)$$

$$d_{43} = \kappa_{d_2} b y_n'(\kappa_{d_2} b)$$

$$d_{44} = n(n+1) j_n(\kappa_{s_2} b)$$

$$d_{45} = n(n+1) y_n(\kappa_{s_2} b)$$

$$d_{46} = -k_{d_3} b j_n'(k_{d_3} b)$$

$$d_{47} = -k_{d_3} b y_n'(k_{d_3} b)$$

$$d_{48} = -n(n+1) j_n(k_{s_3} b)$$

$$d_{49} = -n(n+1) y_n(k_{s_3} b)$$

$$d_{52} = -j_n(\kappa_{d_2} b)$$

$$d_{53} = -y_n(\kappa_{d_2} b)$$

$$d_{54} = -\kappa_{s_2} b j_n'(\kappa_{s_2} b) - j_n(\kappa_{s_2} b)$$

$$d_{55} = -\kappa_{s_2} b y_n'(\kappa_{s_2} b) - y_n(\kappa_{s_2} b)$$

$$d_{56} = j_n(k_{d_1}b)$$

$$d_{57} = y_n(k_{d_3}b)$$

$$d_{58} = k_{s_3}bj_n'(k_{s_3}b) + j_n(k_{s_3}b)$$

$$d_{59} = k_{s_3}by_n'(k_{s_3}b) + y_n(k_{s_3}b)$$

$$d_{62} = \frac{1}{\mu_{e_3}}(\mu_{e_2} - i\omega\mu_{v_2})\{-4\kappa_{d_2}bj_n'(\kappa_{d_2}b) + [2n(n+1) - \kappa_{s_2}^2b^2]j_n(\kappa_{d_2}b)\}$$

$$d_{63} = \frac{1}{\mu_{e_3}}(\mu_{e_2} - i\omega\mu_{v_2})\{-4\kappa_{d_2}by_n'(\kappa_{d_2}b) + [2n(n+1) - \kappa_{s_2}^2b^2]y_n(\kappa_{d_2}b)\}$$

$$d_{64} = \frac{2n(n+1)}{\mu_{e_3}}(\mu_{e_2} - i\omega\mu_{v_2})[\kappa_{s_2}bj_n'(\kappa_{s_2}b) - j_n(\kappa_{s_2}b)]$$

$$d_{65} = \frac{2n(n+1)}{\mu_{e_3}}(\mu_{e_2} - i\omega\mu_{v_2})[\kappa_{s_2}by_n'(\kappa_{s_2}b) - y_n(\kappa_{s_2}b)]$$

$$d_{66} = 4k_{d_3}bj_n'(k_{d_3}b) - [2n(n+1) - k_{s_3}^2b^2]j_n(k_{d_1}b)$$

$$d_{67} = 4k_{d_3}by_n'(k_{d_3}b) - [2n(n+1) - k_{s_3}^2b^2]j_n(k_{d_3}b)$$

$$d_{68} = 2n(n+1)[j_n(k_{s_3}b) - k_{d_3}bj_n'(k_{s_3}b)]$$

$$d_{69} = 2n(n+1)[y_n(k_{s_3}b) - k_{s_3}by_n'(k_{s_3}b)]$$

$$d_{72} = 2[j_n(\kappa_{d_2}b) - \kappa_{d_2}bj_n'(\kappa_{d_2}b)]$$

$$d_{73} = 2[y_n(\kappa_{d_2}b) - \kappa_{d_2}by_n'(\kappa_{d_2}b)]$$

$$d_{74} = 2\kappa_{s_2}bj_n'(k_{s_2}b) + [\kappa_{s_2}^2b^2 - 2n(n+1) + 2]j_n(\kappa_{s_2}b)$$

$$d_{75} = 2\kappa_{s_2}by_n'(\kappa_{s_2}b) + [\kappa_{s_2}^2b^2 - 2n(n+1) + 2]y_n(\kappa_{s_2}b)$$

$$d_{76} = -\frac{2\mu_{e_3}}{\mu_{e_2} - i\omega\mu_{v_2}}[j_n(k_{d_3}b) - k_{d_3}bj_n'(k_{d_3}b)]$$

$$d_{77} = -\frac{2\mu_{e_3}}{\mu_{e_2} - i\omega\mu_{v_2}}[y_n(k_{d_3}b) - k_{d_3}by_n'(k_{d_3}b)]$$

$$d_{78} = -\frac{\mu_{e_3}}{\mu_{e_2} - i\omega\mu_{v_2}}\{2k_{s_3}bj_n'(k_{s_3}b) + [k_{s_3}^2b^2 - 2n(n+1) + 2]j_n(k_{s_3}b)\}$$

$$d_{79} = -\frac{\mu_{e_3}}{\mu_{e_2} - i\omega\mu_{v_2}}\{2k_{s_3}by_n'(k_{s_3}b) + [k_{s_3}^2b^2 - 2n(n+1) + 2]y_n(k_{s_3}b)\}$$

$$d_{86} = -4k_{d_3}aj_n'(k_{d_3}a) + [2n(n+1) - k_{s_3}^2a^2]j_n(k_{d_3}a)$$

$$d_{87} = -4k_{d_3}ay_n'(k_{d_3}a) + [2n(n+1) - k_{s_3}^2a^2]y_n(k_{d_3}a)$$

$$d_{88} = -2n(n+1)[j_n(k_{s_3}a) - k_{s_3}aj_n'(k_{s_3}a)]$$

$$d_{89} = -2n(n+1)[y_n(k_{s_3}a) - k_{s_3}ay_n'(k_{s_3}a)]$$

$$d_{8,10} = \frac{\rho_4}{\rho_3}k_{s_3}^2a^2j_n(k_4a)$$

$$d_{96} = k_{d_3}aj_n'(k_{d_3}a)$$

$$d_{97} = k_{d_3}ay_n'(k_{d_3}a)$$

$$d_{98} = n(n+1)j_n(k_{s_3}a)$$

$$d_{99} = n(n+1)y_n(k_{s_3}a)$$

$$d_{9,10} = -k_4aj_n'(k_4a)$$

$$d_{10,6} = 2[j_n(k_{d_3}a) - k_{d_3}aj_n'(k_{d_3}a)]$$

$$d_{10,7} = 2[y_n(k_{d_3}a) - k_{d_3}ay_n'(k_{d_3}a)]$$

$$d_{10,8} = 2k_{s_3}aj_n'(k_{s_3}a) + [k_{s_3}^2a^2 - 2n(n+1) + 2]j_n(k_{s_3}a)$$

$$d_{10,9} = 2k_{s_3}ay_n'(k_{s_3}a) + [k_{s_3}^2a^2 - 2n(n+1) + 2]y_n(k_{s_3}a)$$

and finally,

$$A_1^{\dagger} = -\frac{\rho_1}{\rho_2}\kappa_{s_2}^2c^2j_n(k_1c), \quad A_2^{\dagger} = k_1cj_n'(k_1c).$$

As given here, all these elements are not only non-dimensionalized, but also they have been reduced to their simplest forms. Note that they depend only on the spherical Bessel (or Neumann or Hankel) functions, and at most on their first derivatives.